CrystEngComm

Potential for improved transport in core-shell $CuInS_2$ nanoparticle solar cells from an Ag surface termination

Journal:	*CrystEngComm*
Manuscript ID	CE-ART-05-2018-000728
Article Type:	Paper
Date Submitted by the Author:	04-May-2018

Complete List of Authors:	Hu, Yicong; UNSW, School of Photovoltaic and Renewable Energy Engineering Patterson, Rob; UNSW, School of Photovoltaic and Renewable Energy Engineering Chin, Robert; University of New South Wales, School of Photovoltaic and Renewable Energy Zheng, Jianghui; University of New South Wales, School of Photovoltaic and Renewable Energy Song, Ning; University of New South Wales, School of Photovoltaic and Renewable Energy Engineering Hu, Long; UNSW, School of Photovoltaic and Renewable Energy Engineering Conibeer, Gavin; University of New South Wales, Huang, Shujuan; University of New South Wales, ARC centre of excellence

CrystEngComm

FULL PAPER

Potential for improved transport in core-shell $CuInS_2$ nanoparticle solar cells from an Ag surface termination

aReceived 00t h January 20xx,
Accepted 00th January 20xx

DOI: 10.1039/x0xx00000x

www.rsc.org/

Yicong Hu,[a] Rob Patterson,*[a] Robert Lee-Chin,[a] Jianghui Zheng,[a] Ning Song,[a] Long Hu,[a] Gavin Conibeer,[a] Shujuan Huang[a]

A major factor limiting the performance of nanostructured $CuInS_2$ photovoltaic devices is the current density, pointing to poor charge carrier transport in $CuInS_2$ nanoparticle films. In a typical $CuInS_2$ core/shell structure synthesis, ZnS is typically chosen as a shell material for $CuInS_2$ core passivation, which leads to a significant enhancement of the photoluminescence quantum yield from the $CuInS_2$ nanoparticles. While typically a marker for excellent photovoltaic performance, in this case the increased photoluminescence likely signals increased charge carrier confinement and reduced transport through any thin films fabricated from the nanoparticles. Here we show that replacing the typical divalent Zn cation surface termination with a monovalent Ag cation leads to small improvements in charge carrier transport through nanostructured films. This surface termination intentionally introduces lower energy electronic states directly at the surface of the $CuInS_2$ nanoparticles, reducing charge carrier confinement and thus increasing charge carrier mobility between nanoparticles. The study assessed appropriate Ag molar ratios to be used in synthesis, with an 8% Ag:Cu ratio found to be optimal. The passivation offered by an Ag surface termination appears comparable to that from Zn with strong photoluminescence observed in both cases. Slight improvements in the performance of all-solid-state nanoparticle $CuInS_2$ photovoltaic devices are obtained, with current densities in the Ag surface terminated case being increased by just under 10%. These findings outline a potential strategy for the synthesis of type II core-shell $CuInS_2$ quantum dot thin film devices with improved charge transport.

[a] *School of Photovoltaic and Renewable Energy Engineering, University of New South Wales, Sydney Australia 2033.*

CrystEngComm

FULL PAPER

1. Introduction

The $CuInS_xSe_{2-x}$ material system has shown excellent performance in both physically deposited thin films [1-4] and nanoparticle sensitized photovoltaic structures employing thick mesoporous TiO_2, [5] with efficiencies in sensitized device structures of over 11% having been demonstrated. However, relative to these results, so-called planar structure nanoparticle solar cells remain unoptimized with maximum efficiencies of fully solution processed cells having reached only 1.5%.[1] Open circuit voltage (V_{oc}) values in the planar structures are quite competitive, being on the order of 0.6 or 0.7 eV.[1] However short circuit current density (J_{sc}) values lag considerably behind state of the art PbS planar structures, which typically are on the order of 25 mA/cm^2 [6], and nanoparticle $CuInS_2$-sensitized solar cells having current densities of a similar magnitude.[5, 7] In the sensitized case, charge separation across the $CuInS_2$ nanoparticle and transport to the mesoporous TiO_2 and the polysulfide electrolyte solution occurs across a few nanometers, whereas in the case of the planar structure transport through a relatively thick $CuInS_2$ nanoparticle film spanning a few hundred nanometers is required in order to achieve optimal light absorption. This suggests that charge transport through $CuInS_2$ nanoparticle thin films is the limiting factor to achieving efficiency improvements in planar photovoltaic devices based on this material.

$CuInS_2$ is known to have a relatively small Bohr radius of 4.1 nm,[8] similar to that of silicon.[9] This may be an intrinsic problem for transport in liganded nanoparticle thin films, though related materials such as $AgBiS_2$ also have small Bohr radii and show reasonable photovoltaic performance.[10, 11] The properties of bulk $CuInS_2$ are known to be very suitable for photovoltaic applications, with charge carrier lifetimes in the microsecond regime.[12]

Photoluminescence quantum yield (PLQY) is often used as a figure of merit to determine which semiconductors have the potential to yield high efficiency in solar cell applications. To obtain excellent PLQY from $CuInS_2$ nanocrystals typically a surface passivation step to create a thin ZnS shell has been employed.[13, 14] While a core-shell ZnS:$CuInS_2$ structure can give exceptional luminescence efficiencies of up to ~70%,[13] the presence of the wide bandgap shell likely further exacerbates transport problems in all-solid-state solar cell structures. Therefore, it is of interest to find alternative materials that can effectively passivate the surface of $CuInS_2$ nanoparticles without introducing a large potential barrier in this small Bohr radius material system.

Silver compounds have recently been of considerable interest in the solar cell community, with Ag having been used alongside Bi in so-called "double perovskites".[15] Silver alloys are a part of the I-III-VII family of compounds, to which $CuInS_2$ belongs, that includes materials such as $AgBiS_2$, $AgSbS_2$, etc.[16, 17] Pure silver sulphide has been explored previously in solar applications[18] and is known to crystallize in a monoclinic structure with a bandgap of approximately 1 eV.[19] Silver is also a larger, heavier atom than both Cu and Zn. By simple arguments any substitutional effects Ag may have in the material have some possibility of increasing the Bohr radius of electronic states that participate in inter-particle transport, particularly near the surface.

Here, we report an initial investigation into the potential replacement of the typical ZnS shell with an Ag surface termination on $CuInS_2$ nanoparticles (Ag:$CuInS_2$), in an effort to improve transport through compact $CuInS_2$ nanoparticle thin films. Figure 1 shows a schematic diagram of the bulk band offsets for ZnS:$CuInS_2$ and Ag_2S:$CuInS_2$ in a core-shell structure. While a ZnS surface termination provides an approximately 1 eV barrier for electrons and holes, an Ag surface termination nominally extracts electrons and holes to the surface for transport. The synthesis recipe for Ag:$CuInS_2$ is a modified method based on state of the art syntheses for $CuInS_2$ with ZnS.[7, 20-22] It was found that Ag:$CuInS_2$ does indeed show significant photoluminescence (PL), suggesting that surface defects are suppressed through the application of a thin Ag surface termination on the $CuInS_2$ nanocrystals despite the potentially lower bandgap of the surface terminating layer. Solar cells were fabricated using the Ag:$CuInS_2$ and slight improvements in transport were observed. This suggests that with further optimization an Ag surface treatment on $CuInS_2$ nanoparticles could lead to significant improvements in all-solid-state, low temperature solution processed nanoparticle solar cells in this high performance material system.

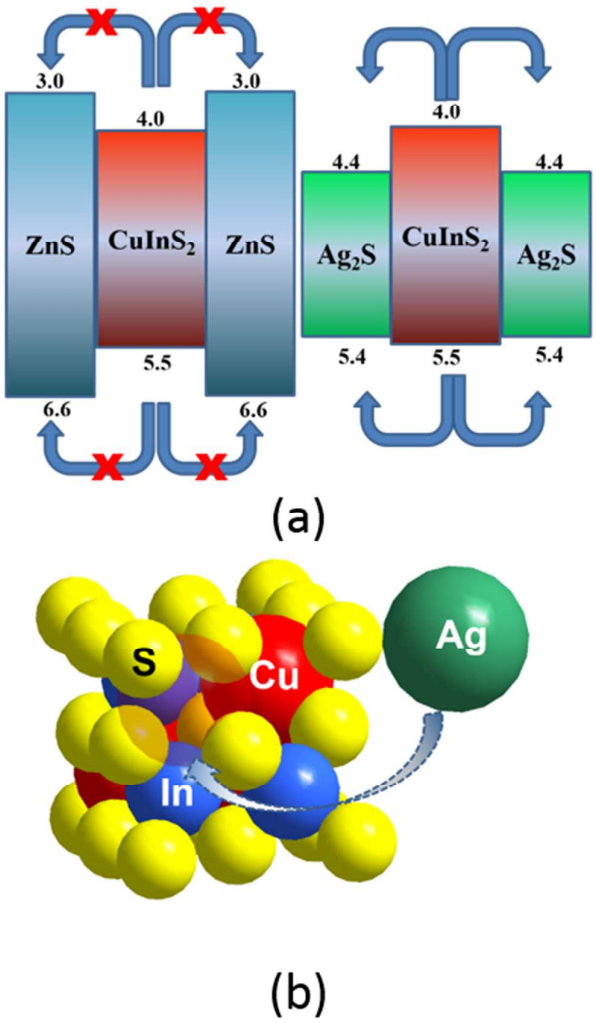

Figure 1. The bulk band offsets and barrier heights for $ZnS:CuInS_2$ core-shell nanoparticles as well as the expected band offsets for $Ag_2S:CuInS_2$ nanoparticles. No barriers to inter-particle charge carrier transport exist in the $Ag_2S:CuInS_2$ case. (b) Schematic diagram showing monovalent Ag cation surface termination on the $CuInS_2$ surface.

2. Experimental

2.1 Nanoparticle synthesis

$CuInS_2$ nanoparticles were fabricated according to a recipe published previously.[21] A mixture of 0.8 mmol CuI and 1 mmol indium acetate in 7.5 mL of trioctylphosphine (TOP), 9 mL of oleylamine (OLA) and 15 mL of octadecene (ODE) was degassed in a three-necked flask for 30 mins, heated and stirred until dissolution at 100°C for another 30 mins under vacuum. A clear solution was obtained after approximately the first 10 minutes of stirring. Then the temperature of the solution was raised to 170°C. Hot injection at this temperature was performed using 310 µL of bis(trimethylsilyl)sulfide (TMS) as a sulphur source. The TMS had been dissolved in 7.5 mL of ODE that had been degassed prior to its dissolution. On injection, the solution immediately cooled to 150°C and the heater power to the reaction vessel is adjusted to maintain this temperature for 15 minutes to grow the nanoparticles. During the growth phase the colour of the solution changed from clear to yellow then red and finally black over a few seconds. Then the reaction was finished by quenching the flask in an ice bath. The product was recovered by centrifugation at 3500 rpm for 5 minutes using 5 mL of toluene to resuspend the nanoparticles and 70 mL of absolute ethanol as an anti-solvent in 5 separate centrifuge tubes. The centrifugation steps were repeated only once before ligand exchange to prevent excessive removal of the surface ligands. Finally the nanoparticles were suspended in 6 mL of toluene.

The shell precursor in an amount of 1 mmol for Zn acetate and amounts between 0.0625 mmol and 0.25 mmol for Ag acetate were dissolved in 3 mL oleic acid (OLAc) and 6 mL ODE and then degassed at 80°C for 30 mins. The $CuInS_2$ nanoparticle solution was then injected into this shell precursor solution and left to react for 30 minutes at 80°C. The solution was again quenched using a water bath. The nanoparticles were then purified via the following centrifugation steps. The nanoparticles were suspended in 5 mL of toluene and 40 mL of acetone as a solvent and anti-solvent respectively. The solution was purified by centrifugation once at 3500 rpm for 5 minutes. Then 4 mL of toluene and 10 mL of methanol were used as the solvent and anti-solvent and the centrifugation was repeated. Then the solvent amounts were reduced to 2 and 5 mL respectively and centrifugation repeated. This product was dissolved in 2 mL of toluene and centrifuged at 3500 rpm for 5 minutes and the supernatant was collected, with any precipitates discarded. The nanoparticles were finally resuspended in toluene with a final concentration of about 80 mg/mL.

2.2 Device fabrication

A compact TiO_2 layer was deposited on a pre-cleaned FTO coated glass substrate (Pilkington, 14 ohms/square) by a spray coating and annealing method using an ethanolic solution of Ti-isopropoxide as the Ti precursor [23]. The spray coating was then dried on a hotplate at 150°C for 5 minutes. A mesoporous TiO_2 layer was then deposited on top of the compact layer by spin coating (3000 rpm, 30 s) a commercial TiO_2 paste (90T) from Dyesol (GreatCell) at a volume ratio of 1:6 paste to ethanol respectively. The mesoporous TiO_2 film was then annealed at 500°C for 30 mins with a ramp rate of 40°C/min and allowed to cool naturally to room temperature.

Thin films of $CuInS_2$ nanoparticles were spin-coated on top of the previously deposited TiO_2 films at 3000 rpm for 30 seconds using a Laurell spin coater from the colloidal solutions

described above. Solid state ligand exchange to link the nanoparticles was performed using a solution containing 2 vol% formic acid in methanol according to the method from Konstantatos's.[21] Spin-coated films were rinsed using methanol and toluene between deposition and linking steps. The nanoparticle deposition procedure was repeated 18 times. Then a layer of 2,2',7,7'-tetrakis(N,N-di-pmethoxyphenylamine)-9,9-spirobifluorene (Spiro-OMeTAD) was deposited as a hole transporting layer (HTL) by spin-coating a Spiro-OMeTAD solution at 3000 rpm. The solution was prepared by dissolving 72.3 mg Spiro-OMeTAD , 31.2 µL, 4-tertbutylpyridine and 17.4 µL lithium bis(trifluoromethylsulphonyl)imide solution (520 mg/mL in acetonitrile) in 1 mL chlorobenzene. Finally Au contacts were evaporated onto the back surface of the device.

2.3 Characterisation

Transmission electron microscopy (TEM) was performed on the nanoparticles using a Phillips CM200. Scanning electron microscopy (SEM) images were taken using a field emission SEM (NanoSEM 230). X-ray diffraction (XRD) patterns were measured using the Empyrean thin film Xpert Materials Research diffractometer system with a triple axis goniometer and analysed using standard High Score plus software. Raman scattering on drop-cast films was measured on an Invia microRaman system at an excitation wavelength of 532 nm. The PL of the suspended $CuInS_2$ colloid was measured on a micro-PL system also at an excitation wavelength of 532 nm. The current density–voltage (*J–V*) measurements were made using a solar cell testing system from Abet Technologies, Inc. (using class AAA solar simulator) under an illumination power of 100 mW cm^{-2}.

Results and Discussion

In most cases knowledge of the precise role that the new atomic species (Zn or Ag) plays in the shell formation is not clear and in principle many possible locations for these atoms in the final material are possible. The additional atoms may bond to exposed surface sulphur, may diffuse into the material or perform some kind of substitution through cation exchange (eg. In and Cu) and may also grow into legitimate shells with relatively well defined interfaces. Clearly there is a dependence on growth time and temperature in the final atomic configuration and to some degree all three mechanisms can be expected to participate in this relatively complicated quaternary material system.

Figure 2 shows XRD data from syntheses of Ag:$CuInS_2$ nanoparticles for different times and initial Ag precursor concentrations at a fixed temperature of 80°C. Small concentrations of Ag introduced into the reaction vessel do not appear to lead to measurable formation of a secondary material phase that is separate from the $CuInS_2$ nanoparticles. This also appears to be true for short annealing times at a fixed initial precursor amount of 0.0625 mmol. This is consistent with the Ag attaching onto the surface of the $CuInS_2$ nanoparticles as nucleation points for further material growth, without introducing a new crystal phase (surface termination or very thin shell formation). For longer growth times and higher concentrations with the Ag precursor present, XRD peaks corresponding to the formation of a new phase of pure Ag_2S are evident. A concentration of 0.125 mmol and growth time of 30 minutes appear not to lead to the formation of the secondary Ag_2S phase. XRD peaks from $CuInS_2$ remain in the XRD results on the growth of the secondary phase, though they grow weaker for large Ag-precursor concentrations and longer growth times. For small amounts of the Ag-precursor, limited or no phase segregation or additional phases are visible in the XRD. This is consistent with a very thin Ag surface termination on the $CuInS_2$ nanoparticles. This also appears to be true for relatively short growth times at low concentrations of the Ag precursor. For long growth times or high concentrations of the Ag precursor, the new Ag_2S phase is clearly evident. This is consistent with both cation exchange to produce an Ag_2S shell on $CuInS_2$ nanoparticles or the consumption of the sulphur in $CuInS_2$ to produce phase segregated Ag_2S nanoparticles. JCPDS cards for $CuInS_2$ and monoclinic Ag_2S are also shown in Figure 2 for comparison to the XRD spectra.

We also observed that the stability of the colloid was greatly improved by the introduction of a shell, with time periods before agglomeration increasing from several days for uncoated $CuInS_2$ to months for Zn:$CuInS_2$ and Ag:$CuInS_2$.

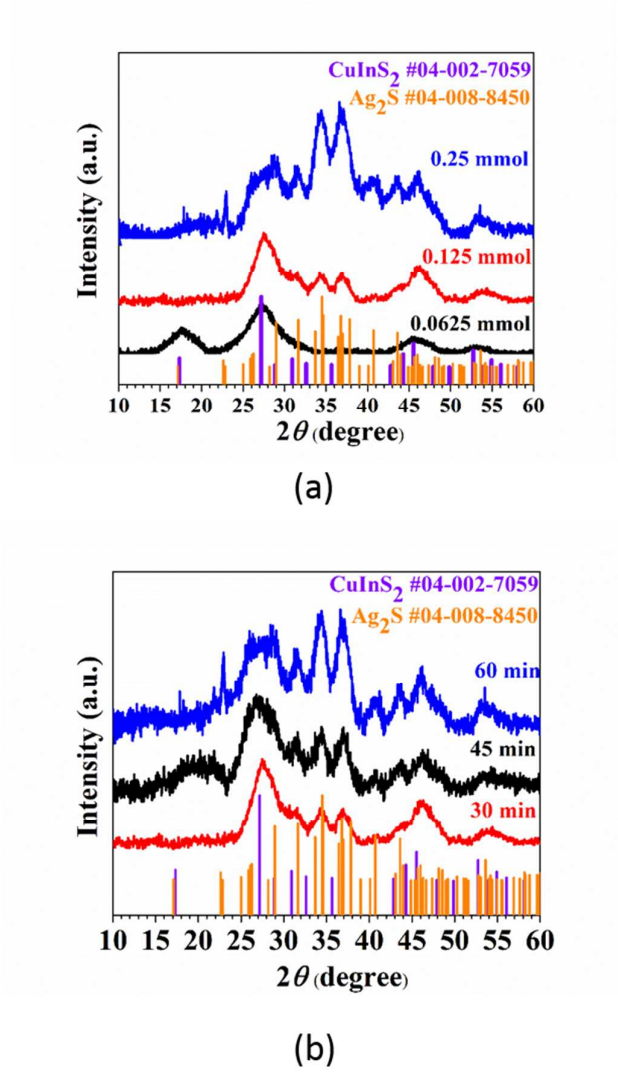

Figure 2. XRD results for Ag:$CuInS_2$ nanoparticles synthesized by the recipe described in Ref 24 and modified for Ag, (a) using different initial amounts of the Ag-precursor from 0.0625 mmol to 0.25 mmol and synthesis times of 30 mins, (b) having different growth times at a constant Ag-precursor concentration of 0.125 mmol.

To assess phase segregation, TEM microscopy of the optimal synthesis was performed, looking for changes in the particle morphology. Figure 3(a) to 3(b) show the TEM images of the $CuInS_2$ nanoparticles for two Ag-precursor amounts and growth periods. For high Ag precursor concentrations of 0.25 mmol (Figure 3b) a distinct change in the morphology of the particles was observed. Relatively large "dark" particles having significant increases in beam scattering appeared in the final colloid that was obtained, as shown in Figure 3 (b). Longer growth times at ~80°C did not lead to this same particle morphology, consistent with the formation of an Ag surface termination (Figure S1a). The XRD results exclude the possibility that this new phase is an Ag-Cu-In-S alloy or solid solution, which would have been possible for significant internal diffusion of the surface terminating cation. Longer growth periods at high temperature lead to more of the secondary, segregated Ag_2S phase being formed. As seen in Figure 3(b, inset), dimer-like nanoparticles appear in the colloid, in addition to phase segregated particles.

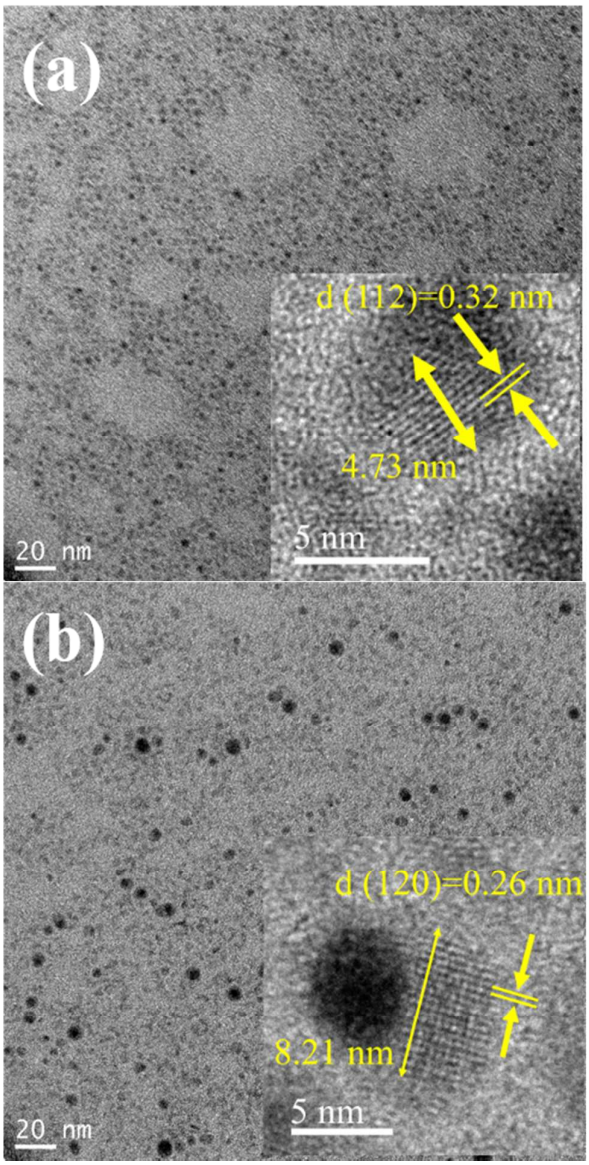

Figure 3. TEM images showing the morphology of Ag:$CuInS_2$ synthesized at 80°C for 30 mins with (a) 0.125 mmol, (b) 0.25 mmol of the Ag precursor. The image in (a) shows the beginning of the formation of the new phase and (b) clearly shows the emergence of a different morphology, attributed to a new Ag_2S phase consistent with the XRD results. The trend with increasing Ag concentration toward the production of these larger particles is clear. The image in (a) inset shows fringe a spacing that match well to the (112) planes in $CuInS_2$. In (b) the inset shows a fringe spacing consistent with the (120) plane of Ag_2S, again consistent with the XRD results.

Figure 4 shows a comparison between the photoluminescence (PL) and absorption spectrum obtained from an Ag:$CuInS_2$

sample, fabricated with 0.125 mmol of silver precursor and a growth time of 30 mins such that secondary Ag_2S phases should not form, and a ZnS:$CuInS_2$ (Zn:$CuInS_2$) sample fabricated following Ref 21. The main PL peak compares well with the onset of the absorption in both the Zn and Ag terminated cases and can be attributed to band-to-band luminescence from a $CuInS_2$ core at approximately 1.70 eV for Zn and 1.65 eV in the Ag terminated cases. However, complex PL with many shoulders and sub-peaks are observed. For small amounts of shell species (Zn or Ag), these are consistent with various degrees of surface coverage and alloying in the overall group of nanoparticles. Some $CuInS_2$ nanoparticles may have slightly higher degrees of penetration of the shell species into the core regions, forming shallow defect levels. The insets in Figure 3(a) and (b) show higher magnification TEM images of individual nanoparticles and show that the nanoparticles may not be single crystalline. Some regions of the nanoparticle show crystalline fringes while others do not. This is consistent with the PL results. Small bandgap increases relative to the bulk $CuInS_2$ material may result from a small contribution from quantum confinement effects for the 3 nm diameter nanoparticles. At least two low energy shoulders are visible in the PL spectra, showing that these nanostructures likely have more than one radiative shallow electronic state. The low energy shoulder centred at approximately 1.5 eV may be introduced by an Ag-S surface state, as this shoulder appears to move to higher energies (~1.6 eV) in the Zn terminated case. The Zn:$CuInS_2$ peak is also visibly asymmetric, likely indicating appreciable radiative transitions from shallow states. Any Ag-S states at the surface may be expected to have slightly lower energies since to the bulk bandgap of Ag_2S is measurably lower than that of $CuInS_2$, at 1.0 eV. This may also contribute to the slight decrease in the PL peak location in the Ag-terminated case relative to the Zn-terminated one. That transitions from shallow defect states are radiative suggests long lifetimes for carriers occupying these states and that the Ag surface termination has provided reasonably good passivation. In fact, though the peaks shown in Figure 4 are normalized for comparison, the Ag:$CuInS_2$ colloid showed almost an order of magnitude higher PL intensity than did the Zn:$CuInS_2$ material, for comparable fabrication conditions and the same nanoparticle concentration.

The Raman data in Figure 4 (b), after a synthesis with 0.125 mmol of the Ag precursor and 30 mins of growth time, show that the $CuInS_2$ core is still intact, corresponding well with XRD data. This provides further evidence of the Zn and Ag treatments indeed terminating the surface of the nanoparticles and that any alloying is minimal for a synthesis method that does not produce secondary phases.

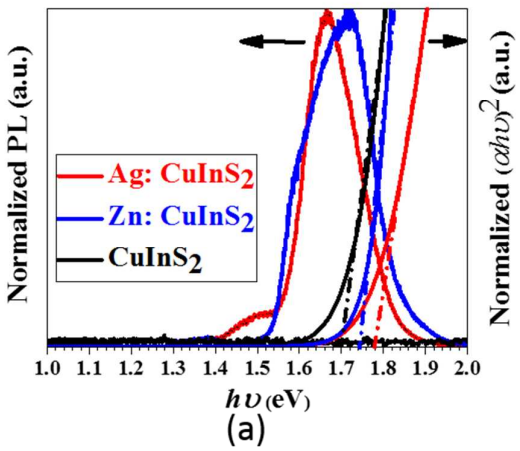

Figure 4. Comparison of Ag:$CuInS_2$ nanoparticles and Zn:$CuInS_2$ nanoparticles: (a) PL and absorption as well as (b) Raman spectra. In the PL, a clear peak for both materials that matches well with the onset of the absorption was observed, implying luminescence from the $CuInS_2$ core. The Raman data shown in (b) corresponds to $CuInS_2$[25] and demonstrates that despite exposure to the different metal ion, Zn or Ag, the core $CuInS_2$ phase appears to be intact after the synthesis with 0.125 mmol Ag precursor and 30 mins growth time.

Figure 5 shows the *J-V* curves of solar cells made from an optimal Zn:$CuInS_2$ and Ag:$CuInS_2$ nanoparticles, using 0.125 mmol of the surface terminating precursor and a 30 min growth time. Typical for these materials, the V_{oc} values are quite reasonable at 0.6 to 0.7 eV. However, the current densities are low, similar to the results shown by Konstantatos and well below those obtained from a sensitized structure. [1, 7, 21] Cells fabricated in this work show that the use of Ag:$CuInS_2$ nanoparticles slightly improve the J_{sc}, suggesting improved transport through the film. However, fill factors (FF) appear to suffer with the introduction of the Ag, which may be a consequence of the relatively deep surface states induced by Ag surface termination as visible in the PL data. Surprisingly, despite terminating the surface with a nominally lower bandgap material, V_{oc} values remain comparable to Zn:$CuInS_2$ devices. This is consistent with the $CuInS_2$ core determining the overall optoelectronic properties of the material, such as the splitting in quasi-Fermi levels. This also suggests that band

offsets and doping levels are similar in the Ag and Zn cases, which is interesting due to the significantly different energetics they could be expected to contribute at the nanoparticle's surface from the Zn or Ag atoms.

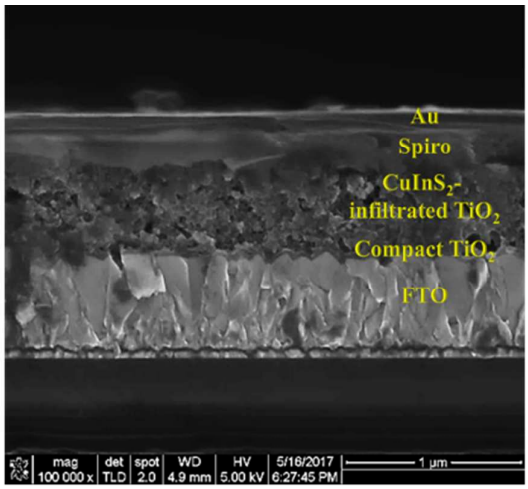

(a)

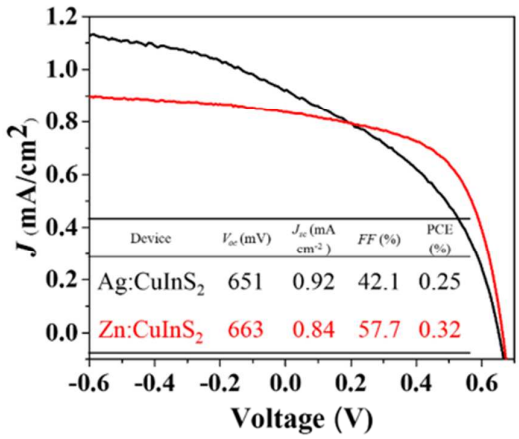

(b)

Figure 5. (a) Cross-sectional SEM image of the layers in the final device. From bottom to top, a bright layer of FTO is visible, followed by a thin ~50 nm thick compact TiO_2 layer. Above that, the $CuInS_2$ nanoparticle layer incorporated into mesoporous TiO_2 is present. Finally, a layer of Spiro-OMeTAD caps the absorber layer before the metal contact layer. (b) J-V curves of Zn:$CuInS_2$ and Ag:$CuInS_2$ solar cells showing a small improvement in the J_{sc} value for films of $CuInS_2$ with an Ag surface termination. Overall efficiencies remain modest, to be compared against results from Refs.[1, 7, 21]

Conclusions

Initial work regarding the synthesis of Ag surface terminated $CuInS_2$ nanoparticles as an improved nanoparticle material for all-solid-state solar energy conversion has been presented. A threshold time and Ag-precursor content in the synthesis, such that secondary phases detrimental to the $CuInS_2$ phase do not form, has been reported. An interesting shallow state is likely present in the Ag:$CuInS_2$, leading to the significant low energy shoulder observed in the PL. This smaller PL peak may be due to radiative transitions from shallow surface states introduced by Ag. Similar charge carrier lifetimes appear to have been obtained from Ag-terminated $CuInS_2$ nanoparticles, with PL intensities equivalent to or larger than the Zn-terminated case observed. In a complete photovoltaic device, slight improvements in short-circuit current density for the Ag:$CuInS_2$ device were obtained. This implies that the passivation from an Ag surface termination may be comparable to the passivation provided by Zn. With further optimization there is significant potential to improve charge carrier transport in $CuInS_2$ nanoparticle thin films through Ag surface treatments.

Conflicts of interest

There are no conflicts to declare.

Acknowledgements

Yicong Hu gratefully acknowledges funding from the University Postgraduate Award (UPA) scholarship for support. The group thanks the Australian Research Council (ARC) Discovery Project scheme (DP140102073) and the University of New South Wales (UNSW) Silver Star Award for supporting the work.

Notes and references

1. J. E. Halpert, F. S. Morgenstern, B. Ehrler, Y. Vaynzof, D. Credgington and N. C. Greenham, *ACS Nano*, 2015, 9, 5857-5867.
2. M. S. Stahl, H. Azimi and C. J. Brabec, *J. Mater. Chem. A*, 2015, 3, 14116-14120.
3. A. Uhl, J. Katahara and H. Hillhouse, *Energy Environ. Sci*. 2016, 9, 130-134.
4. B.-S. Lee, Y. Hwang, H. N. Pham, J. Y. Kim, M. H. Song and D.-K. Lee, *J. Mater. Chem. A*, 2015, 3, 15889-15896.
5. J. Du, Z. Du, J.-S. Hu, Z. Pan, Q. Shen, J. Sun, D. Long, H. Dong, L. Sun and X. Zhong, *J. Am. Chem. Soc.*, 2016, 138, 4201-4209.
6. M. Liu, O. Voznyy, R. Sabatini, F. Arquer, R. Munir, A. H. Balawi, X. Lan, F. Fan, G. Walters and A. R. Kirmani, *Nat. Mater.*, 2017, 16, 258-263.
7. Z. Pan, I. n. Mora-Seró, Q. Shen, H. Zhang, Y. Li, K. Zhao, J. Wang, X. Zhong and J. Bisquert, *J. Am. Chem. Soc.*,2014, 136, 9203-9210.

8. C. Czekelius, M. Hilgendorff, L. Spanhel, I. Bedja, M. Lerch, G. Müller, U. Bloeck, D.-S. Su and M. Giersig, *Adv. Mater.*, 1999, 11, 643-646.
9. L. T. Canham, *Appl. Phys. Lett.*, 1990, 57, 1046-1048.
10. M. Bernechea, N. C. Miller, G. Xercavins, D. So, A. Stavrinadis and G. Konstantatos, *Nat. Photon.*, 2016, 10, 521-525.
11. P.-C. Huang, W.-C. Yang and M.-W. Lee, *J. Phys. Chem. C*, 2013, 117, 18308-18314.
12. P. J. Whitham, A. Marchioro, K. E. Knowles, T. B. Kilburn, P. J. Reid and D. R. Gamelin, *J. Phys. Chem. C*, 2016, 120, 17136-17142.
13. Z. Bai, W. Ji, D. Han, L. Chen, B. Chen, H. Shen, B. Zou and H. Zhong, *Chem. Mater.,* 2016, 28, 1085-1091.
14. H. Zang, H. Li, N. S. Makarov, K. A. Velizhanin, K. Wu, Y.-S. Park and V. I. Klimov, *Nano Lett.,* 2017, 17, 1787-1795.
15. F. Giustino and H. J. Snaith, *ACS Energy Lett.,* 2016, 1, 1233-1240.
16. M. Bernechea, N. C. Miller, G. Xercavins, D. So, A. Stavrinadis and K. Konstantatos, *Nat. Photon.,* 2016, 10, 521-525.
17. J. Capistrán-Martínez, M. Nair and P. Nair, *MRS Online Proceedings Library Archive*, 2014, 1670.
18. C. Ji, Y. Zhang, X. Zhang, P. Wang, H. Shen, W. Gao, Y. Wang and W. Y. William, *Nanotechnology*, 2017, 28, 065602.
19. Y. Du, B. Xu, T. Fu, M. Cai, F. Li, Y. Zhang and Q. Wang, *J. Am. Chem. Soc.,* 2010, 132, 1470-1471.
20. F. Meinardi, H. McDaniel, F. Carulli, A. Colombo, K. A. Velizhanin, N. S. Makarov, R. Simonutti, V. I. Klimov and S. Brovelli, *Nat. Nanotechnol.,* 2015, 10, 878-885.
21. D. So, S. Pradhan and G. Konstantatos, *Nanoscale*, 2016, 8, 16776-16785.
22. L. Li, T. J. Daou, I. Texier, T. T. Kim Chi, N. Q. Liem and P. Reiss, *Chem. Mater.,* 2009, 21, 2422-2429.
23. J. Zheng, M. Zhang, C. Lau, X. Deng, J. Kim, Q. Ma, C. Chen, M. Green, S. Huang, A. Baillie, *Solar Energy Materials & Solar Cells*, 2017, 168, 165-171.
24. L. Li, A. Pandey, D. J. Werder, B. P. Khanal, J. M. Pietryga and V. I. Klimov, *J. Am. Chem. Soc.,* 2011, 133, 1176-1179.
25. L. Shi, P. Yin, L. Wang and Y. Qian, *CrystEngComm*, 2012, 14, 7217-7221.

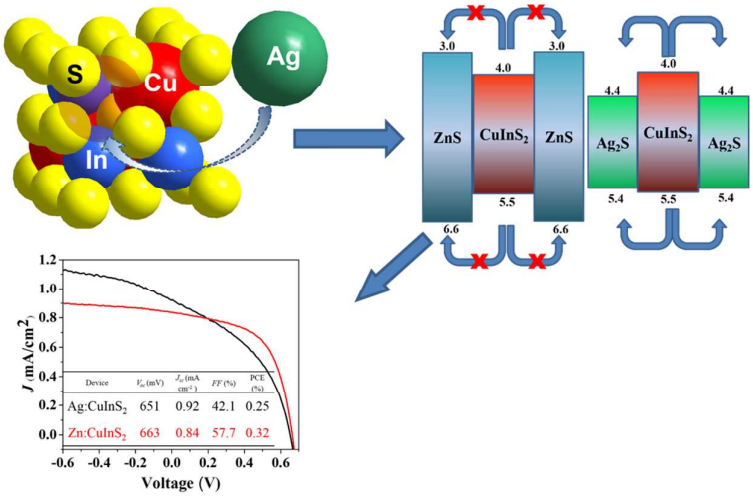

Improvements in charge carrier transport and equivalent photoluminescence were obtained for $CuInS_2$ nanoparticles with an Ag-surface termination in photovoltaic devices.